UNCLASSIFIED

SECURITY CLASSIFICATION OF THIS PAGE *(When Data Entered)*

REPORT DOCUMENTATION PAGE	READ INSTRUCTIONS BEFORE COMPLETING FORM

1. REPORT NUMBER	2. GOVT ACCESSION NO.	3. RECIPIENT'S CATALOG NUMBER
ARO 22886.1-MS	N/A	N/A

4. TITLE *(and Subtitle)*	5. TYPE OF REPORT & PERIOD COVERED
The Determination of Interfacial Tension by Video Image Processing of Pendant Fluid Drops	Technical Report *
	6. PERFORMING ORG. REPORT NUMBER

7. AUTHOR(s)	8. CONTRACT OR GRANT NUMBER(s)
S. H. Anastasiadis, J.-K. Chen, J. T. Koberstein, A. F. Siegel, J. E. Sohn, J. A. Emerson	DAAG29-85-K-0245

9. PERFORMING ORGANIZATION NAME AND ADDRESS	10. PROGRAM ELEMENT, PROJECT, TASK AREA & WORK UNIT NUMBERS
Princeton University Princeton, NJ 08544	

11. CONTROLLING OFFICE NAME AND ADDRESS	12. REPORT DATE
U. S. Army Research Office Post Office Box 12211 Research Triangle Park, NC 27709	March 7, 1986
	13. NUMBER OF PAGES
	25

14. MONITORING AGENCY NAME & ADDRESS(If different from Controlling Office)	15. SECURITY CLASS. *(of this report)*
	Unclassified
	15a. DECLASSIFICATION/DOWNGRADING SCHEDULE

16. DISTRIBUTION STATEMENT *(of this Report)*

Approved for public release; distribution unlimited.

17. DISTRIBUTION STATEMENT *(of the abstract entered in Block 20, If different from Report)*

NA

18. SUPPLEMENTARY NOTES

The view, opinions, and/or findings contained in this report are those of the author(s) and should not be construed as an official Department of the Army position, policy, or decision, unless so designated by other documentation.

19. KEY WORDS *(Continue on reverse side if necessary and identify by block number)*

Polymer Interfacial Tension, Pendant Drop, Image Processing

20. ABSTRACT *(Continue on reverse side if necessary and identify by block number)*

   A novel method for the analysis of interfacial tension from the shape of pendant fluid drops is presented. The experimental apparatus employs digital video image processing techniques to record drop images and to segment the fluid drop profile. An associated drop profile shape analysis algorithm is developed based upon robust shape comparison methods that utilize repeated median concepts. The complete algorithm is designed specifically to be executable on a micro-computer. The performance of the algorithm is illustrated for simulated pendant

DD FORM 1473 EDITION OF 1 NOV 65 IS OBSOLETE   UNCLASSIFIED

SECURITY CLASSIFICATION OF THIS PAGE *(When Data Entered)*

fluid drop profiles and pendant drops of glycerin. In the latter case, the experimental precision in the resultant surface tension is found to be of the order of 0.5%.

Accession For

Dist

A-1

ARo 22886.1-MS

THE DETERMINATION OF INTERFACIAL TENSION

BY VIDEO IMAGE PROCESSING OF PENDANT FLUID DROPS

TECHNICAL REPORT NO. 1

S. H. Anastasiadis, J.-K. Chen, J. T. Koberstein
A. F. Siegel, J. E. Sohn, and J. A. Emerson

MARCH 1986

Introduction

The measurement of interfacial tensions of fluid interphases is a problem of strong current interest for a broad range of scientific disciplines and technologies. As a fundamental parameter, surface tension is the single most accessible experimental parameter that describes the thermodynamic state and structure of an interphase. The technology of interphases is important to a multitude of applications encompassing such diverse areas as coatings, dispersions, adhesion, and membranes to name but a few. It is not surprising then that a great deal of effort has been focussed on the development of methods for measuring interfacial tensions (see references 1-3 for extensive reviews). The most versatile of the available methods are those based on the characterization of axisymmetric fluid drop profiles (2,4-8).

The technique which has found the most widespread usage involves the determination and analysis of pendant fluid drop profiles. The shape of a pendant fluid drop is specified in terms of the cartesian coordinates x and z as depicted in Figure 1, where ϕ is the angle between the horizontal axis and a tangent to the drop profile at position (x,z). The parameter b refers to the radius of curvature at the drop apex and s is the contour length along the profile.

The equations representing this profile can be expressed in dimensionless form (9) as

$$\frac{d\phi}{dS} = \frac{2}{B} + Z\frac{\sin\phi}{X}$$

$$\frac{dX}{dS} = \cos\phi \qquad\qquad [1]$$

$$\frac{dZ}{dS} = \sin\phi$$

where dimensionless reduced variables are defined as $X = x\sqrt{c}$, $Z = z\sqrt{c}$, $S = s\sqrt{c}$, and $B = b\sqrt{c}$.

The dimensionless shape factor is given by

$$B = b\sqrt{c} = b\left(\frac{\Delta\rho g}{\gamma}\right)^{1/2} \qquad [2]$$

where $\Delta\rho$ is the mass density difference between the drop fluid and the surrounding medium, g is the gravitational constant (negative for pendant drops) and γ is the interfacial tension.

Classical methods for the determination of interfacial tension rely on photographic imaging of the drop profile. Characteristic dimensions of the drops are measured manually from enlargements of these photographs, and an estimate of the interfacial tension is furnished by comparison of these dimensions to tabulated theoretical values obtained from numerical solution of [1] (1,10). Although simple in their execution, these methods are limited in accuracy by the necessity for specification of the drop extrema (i.e. position of apex and maximum diameter). In addition, the classical methods can be quite tedious, especially for polymeric systems which require substantial equilibration times.

The pendant drop techique has recently benefitted from a number of advancements both in terms of data acquisition and analysis. The simplest of these improvements makes use of digitizer palettes to efficiently record and store profile coordinates from photographic drop images (11-13). Photographic recording can be eliminated entirely by direct digitization of the drop image with the aid of either a video frame grabber or a direct digital camera (14,15). There are a number of advantages to digital processing of drop images including rapid acquisition, facilitated data manipulation and analysis, and the capabi-

lity for data storage. In addition, the techniques provide a simple means to detect the attainment of equilibrium, a distinct advantage for viscous fluids such as polymer melts. This is accomplished by monitoring the time evolution of the drop profile as it asymptotes towards its equilibrium shape.

The ability to easily detect the entire drop profile has provided an impetus for the concurrent development of sophisticated algorithms for drop profile analysis (14-17). These methods either eliminate or minimize the requirement for specification of extremal drop dimensions, thereby reducing the inherent statistical error. The interfacial tension can be determined by performing a least squares fit of the segmented drop image to the numerical solution of [1]. To date two methods for optimization of this fit have appeared: exhaustive search through the shape parameter B (14); or a sophisticated Newton-Raphson procedure in conjunction with incremental loading (16).

In this communication we describe some further improvements in drop image analysis including a new shape comparison algorithm for the determination of interfacial tensions from axisymmetric fluid drop profiles. The algorithm employs robust shape comparison routines (18-20) which are resistant to outlying points that may result from inaccuracies in the computerized drop profile discrimination procedures. Furthermore, the algorithm is designed to be implemented on a microcomputer, thus enabling routine automation of absolute boundary tension measurements.

Experimental

A block diagram of the experimental apparatus for boundary tension measurements appears in Figure 2. Fluid drops are formed at the tip of either a stainless steel syringe or glass capillary tube which is inserted through a sep-

tum into a quartz cuvette. The cuvette is mounted within a cell with provisions
for both atmosphere and temperature control (±1°C). The optical system consists
of a Unitron microscope (zoom stereo trinocular-ZST) coupled to an RCA model TC
1005 video camera. The optics are focussed by optimizing the video image of a
reticle containing a finely ruled grid that is placed at the drop location. In
addition to furnishing a well defined means for focussing, the grid facilitates
the detection of any image barreling or other distortions that may arise from
the optics, and provides a direct calibration of both the vertical and horizon-
tal magnification factors inherent to the optics and camera systems.

The signal from the video camera is fed to a Tecmar Video Van Gogh board,
which performs the frame grabbing and image digitization. In the high resolu-
tion mode, the image is comprised of a 251 by 255 pixel array with 256 gray
levels. The image analysis software routines are coded in machine language and
Fortran and are executed on an IBM PC.

Drop Profile Analysis

A. Segmentation

The process of drop profile discrimination (i.e. segmentation) is carried
out by applying global thresholding to the drop image. Global thresholding
reduces the 256 gray level image to a binary image by judicious choice of an
appropriate pixel intensity magnitude or threshold. In order to discriminate
the drop interface, the proper threshold magnitude must correspond to an inten-
sity level intermediate between that of the drop and its surrounding medium.
The optimal threshold value is chosen with the aid of a grey level histogram.
Castleman (21) has presented arguments suggesting that the optimal threshold
value is located at the intermediate minimum in the bimodal gray level

histogram. Alternative segmentation techniques, such as adaptive thresholding (21) or gradient magnitude techniques (21-26) could also be adopted. The algebraic operations for these alternative methods require considerable execution time however without substantial improvement in accuracy (under proper lighting conditions) as suggested by Pavlidis (22). Figure 3 shows typical digital images of a pendant drop before thresholding (left), after thresholding (center), and the resultant segmented drop profile (right). A simple test for successful edge detection is superposition of this profile on the original drop image.

B. Piece-Wise Rotationally Resistant Smoothing

The resolution of the segmented drop profile is limited by the resolution of the frame grabber as can be seen from Fig. 3 (right). The situation can be improved by the use of higher resolution frame grabbers, but this leads to increases in both the cost and execution time of the instrument. An alternative approach to increase resolution is to convert the integer pixel values of the digitized drop profile coordinates into the appropriate floating point decimal numbers. This can be accomplished by the application of local polynomial regression smoothing methods. The smoothing operations are applied piece-wise (i.e. point-by-point replacement) along the entire drop profile contour to complete the smoothing procedure. Smoothing parameter options include the order of the polynomial smoothing (e.g. quadratic or cubic), the number of contiguous data points in the local target group, and the number of overall smoothing cycles. Smoothing techniques are often subject to overshoot in regions of steep slope such as are encountered in the near-circular shapes of pendant fluid drops. In order to avoid overshoot, a rotationally resistant smoothing routine was developed.

The smoothing algorithm begins by calculating the local slope of an odd number of contiguous points (e.g. 21) by a principle components fit (i.e. linear regression). These "target" points are then rotated using the resultant coordinate transformation matrix such that the slope is zero. In addition, the points may be translated to the origin in order to normalize the magnitudes of the position coordinates. After rotation and translation, smoothing is accomplished by performing a least squares or robust polynomial fit in the new coordinate system. The smoothed profile coordinate (i.e. midpoint of each target group) in the original coordinate system is then obtained by a second application of the coordinate transformation matrix that returns the profile segment to its original position.

C. Shape Fitting

The process of fitting an experimental drop profile to the theoretical shape predicted by [1] involves a five parameter optimization. Three parameters are required for alignment of the drop. They are a rotation angle, an x translation and a z translation. Drop rotation is required in order to align the camera system to the vertical axis of symmetry of the drop. The final two parameters required are the scale or magnification factor of the drop ($\sqrt{c}$; see [1]), and the shape factor, B. The axis of symmetry is determined by minimizing the sum of squared differences between the distances from corresponding "symmetric" points on each side of the drop to the axis of symmetry. In practice, this algorithm is found to be insensitive to drop symmetry due to the near-spherical shape of the drop. It is preferable to eliminate the need for rotation altogether by prealigning the vertical camera axis with the direction of gravity.

The comparison of shapes by robust methods requires establishment of a reference point so that specific points of comparison may be selected. There

are two natural choices for this reference point: the drop apex, or the drop "center" defined as the intersection of the vertical axis of symmetry and the horizontal maximal drop diameter. Points for comparison from the experimental profile are chosen at predetermined intervals along the contour of the drop profile. Corresponding points from the theoretical profile are selected by requiring that the line segment, connecting the point of interest and reference point on the theoretical profile, have the same slope as the corresponding line segment on the experimental profile. Points on both sides of the drop are employed in order to ensure symmetry.

A first estimate of the dimensionless shape parameter, B_0, is obtained from the approximate relation (17)

$$B_0 = \exp[-6.70905 + 15.3002W - 16.44709W^2 + 9.92425W^3 - 2.58503W^4]$$

[2]

where W is the ratio of the local drop diameter (for a plane located at a distance from the drop apex which is equal in magnitude to the maximum drop diameter) to the maximum drop diameter.

The optimal B value is obtained by exhaustive search in the vicinity of B_0. This optimization is accomplished by robust shape comparison routines developed by Siegel and co-workers (18-20). As in all regression problems, the process involves fitting N points (x_i, y_i) from an experimental profile to N homologous points (u_i, v_i) on a theoretical curve. The theoretical points must be rotated by an angle θ, translated by a vector (α, β) and scaled by a factor τ in order to affect this comparison. The transformed theoretical coordinates

$$\begin{pmatrix} u_i' \\ v_i' \end{pmatrix} = \begin{pmatrix} \alpha \\ \beta \end{pmatrix} + \tau \begin{pmatrix} \cos\theta & -\sin\theta \\ \sin\theta & \cos\theta \end{pmatrix} \begin{pmatrix} u_i \\ v_i \end{pmatrix} \qquad [3]$$

are then compared to (x_i, y_i) for each value of the shape factor, B. The value of the shape factor which yields the minimum overall error provides the optimal fit. The interfacial tension is then obtained from the associated optimal scaling factor τ, by recognizing that $\tau = \sqrt{c} = (\Delta\rho g/\gamma)^{1/2}$.

In least squares regression methods, the values of all of the shape parameters (i.e., $\tau, \theta, \alpha, \beta$) must be chosen simultaneously in order to minimize the sum of squared residuals

$$\text{sum} = \sum_{i=1}^{N} [(x_i - u_i')^2 + (y_i - v_i')^2] \qquad [4]$$

In contrast, with robust shape comparison methods, each of the optimal parameter values may be evaluated independently. In the case of the rotation and magnification variables, this is accomplished using the concept of repeated medians (18-20) as represented by the relations.

$$\tilde{\tau} = \underset{i}{\text{med}} \{\underset{j}{\text{med}} \{\tau_{ij}\}\} \qquad [5]$$

where

$$\tau_{ij} = \frac{[(x_j - x_i)^2 + (y_j - y_i)^2]^{1/2}}{[(u_j - u_i)^2 + (v_j - v_i)^2]^{1/2}} \qquad [6]$$

$$\tilde{\theta} = \underset{i}{\text{med}} \{\underset{j}{\text{med}} \{\theta_{ij}\}\} \qquad [7]$$

where θ_{ij} is the rotation required for the vector from point i to point j in the theoretical shape to have the same attitude as the homologous vector in the experimental profile.

The translation parameters are calculated from the simple (non-repeated) medians:

$$\tilde{\alpha} = \underset{i}{med} \ \{x_i - \tilde{\tau}[u_i\cos\tilde{\theta} - v_i\sin\tilde{\theta}]\} \qquad [8]$$

$$\tilde{\beta} = \underset{i}{med} \ \{y_i - \tilde{\tau}[u_i\sin\tilde{\theta} + v_i\cos\tilde{\theta}]\} \qquad [9]$$

The advantages of double median robust techniques over traditional least square regression methods are discussed in references (18-20).

For each B value assumed, the optimal values of τ, θ, α, and β are specified directly by these relations. The overall optimization routine is therefore reduced to an exhaustive search on the shape parameter B. The ultimate best fit, and associated interfacial tension, is determined from the B value which produces the minimum overall error or deviation from the experimental profile. Three distinct types of error may be calculated for this purpose.

$$SR = \frac{1}{FACTOR} \ [\frac{1}{N} \ \underset{i}{\Sigma} \ [(u_i' - x_i)^2 + (v_i' - y_i)^2]^{1/2} \ ]$$

$$SRR = \frac{1}{FACTOR} \ [\frac{1}{N} \ \underset{i}{\Sigma} \ [(u_i' - x_i)^2 + (v_i' - y_i)^2]]^{1/2} \qquad [10]$$

$$TENSE = \frac{1}{FACTOR} \ [\frac{1}{N - 1} \ \underset{i}{\Sigma} \ [[(u_i' - x_i) - (u_{i-1}' - x_{i-1})]^2 +$$

$$[(v_i' - y_i) - (v_{i-1}' - y_{i-1})]^2]]^{1/2}$$

where

$$\text{FACTOR} = [\sum_i (u_i'^2 + x_i^2) - \frac{1}{2N} (\sum_i(u_i' + x_i))^2 + \sum_i (v_i'^2 + y_i^2) -$$

$$\frac{1}{2N} (\sum_i (v_i' + y_i))^2]^{1/2}$$

The term FACTOR normalizes the total error to the overall size of the
object. TENSE is a measure of the "stress" or "tension" required in "deforming"
the theoretical profile so as to fit the experiment, and in some cases is a more
effective measure of shape differences than is the simple root mean square
error, SR. While the root mean square statistic measures the magnitude of the
differences, the tension measures how quickly this difference is changing. The
error SRR is defined in a fashion to be more resistant to outlying points than
the standard sum of squared residual, SR.

D. Results of Simulations

The performance of the shape comparison algorithm was examined by applying
it to simulated pendant drop profiles generated by a Runge-Kutta numerical solu-
tion of [1]. A typical theoretical profile is shown as the solid line in Figure
4, for a dimensionless shape parameter of B = 0.6. In order to simulate the
actual conditions encountered with the pendant drop apparatus, several sources
of error were introduced. The figure at left shows the same profile after
introduction of Gaussian random noise with an average magnitude of error
corresponding to one pixel element (points). The figure at right shows the ori-
ginal theoretical profile (solid line) along with a profile (points) that has
been rotated by one degree to simulate misalignment of the camera and drop pro-
file coordinate systems. This latter profile was generated using the same
Gaussian error distribution as for the former profile, but also includes addi-

tional non-random errors that were added arbitrarily. Non-random errors were added in order to simulate the possible effects of improper edge detection that might occur for images of low contrast.

The smoothing algorithm that incorporates translation of the target points to the origin as well as rotation provided the best performance, especially in regions near the maximum drop diameter. This result may be attributed to the decreased magnitudes of the drop profile coordinates after they are shifted to the origin. A drawback of translation to the origin is the increase in computation time.

The qualitative performance of the smoothing algorithms is demonstrated in Figure 5. It is apparent that the presence of non-random error (righthand figure) induces considerable distortion into the smoothed drop profile in the vicinity of the outlying point. In principle, these effects could be reduced by the application of robust rather than least squares smoothing routines.

The quantitative performance of the shape analysis and smoothing algorithms was assessed by applying them to the simulated data. When the profile was smoothed prior to shape analysis, comparable results were obtained for both choices of reference point (i.e. apex or center). For unsmoothed profiles subject to considerable noise, however, use of the drop center yielded superior results. This latter observation may be easily explained by the fact that the slopes of line segments that define the comparison points are less sensitive to error for the center reference point than for the apex reference point. For highly elongated drops, however, the apex becomes the reference point of choice, since definition of the position of maximum diameter is problematic. In fact, the apex must be chosen as the reference point for drops that do not exhibit a maximum diameter.

The improvement in performance that results from smoothing is illustrated in Figure 6, where the error SR is plotted as a function of the dimensionless shape parameter. The leftmost figure presents results of the analysis applied to the simulated drop profile (B = 0.6) with random Gaussian error. Without smoothing, the minimum error corresponds to a shape parameter of B_{exp} = 0.597. The deviation from the simulated profile decreases (B_{exp} = 0.598) after application of rotationally resistant smoothing. Similar results are obtained from analysis of the profile with non-random errors and rotation (Fig. 6, right). In this case the magnitudes of deviation from the input value (B = 0.6) are larger as might be expected. Analysis of simulated drop profiles for B = 0.5 yielded best fits of B_{exp} = 0.494 (without smoothing), B_{exp} = 0.501 (with rotationally resistant smoothing), and B_{exp} = 0.500 (rotationally resistant smoothing which incorporates translation to the origin), again illustrating an improvement in precision upon smoothing.

The actual precision of the shape analysis algorithm will depend on the shape parameter B, and the number of data points selected for comparison. The magnitude of the error can be reduced by smoothing and is a function of the order chosen for the polynomial smoothing function, the number of target points for smoothing, and the total number of smoothing cycles. Each improvement in precision however is necessarily accompanied by an associated increase in computation time.

In most simulations, the error curves (e.g. Fig. 6) exhibited discontinuities near the optimal values of B. In a number of these simulations, the least squares algorithm of Rotenberg et al. (11,16) failed to converge when applied to the data. The occurrence of this discontinuity in error may also be

the underlying reason that their algorithm often fails to converge if a non-zero

initial shape parameter estimate (i.e. B_0) is used, since the algorithm requires

a continuous error function for the Newton-Raphson method to function properly.

Experimental Application to the Surface Tension of Glycerin

The shape analysis algorithm was applied to the determination of the

surface tension of glycerin in order to assess its performance under normal

experimental conditions. The density difference $\Delta\rho$ for glycerin was estimated

from density and vapor pressure data tabulated in Perry's handbook (27). For

glycerin at room temperature (24.2 ±0.2°C) the vapor/liquid density difference

was calculated to be $\Delta\rho$ = 1.1745 g/cm^3. The results obtained from analysis of

four pendant drop experiments gave a value of 62.6 ±0.3 dynes/cm for the room

temperature surface tension of glycerin. This compares well with the literature

value of 63.4 dynes/cm (28) reported for a slightly lower temperature (20°C).

The analysis of these drops was performed using 21 data points for the shape

comparison. The correspondence of the fitted profile to these data points and

to the original digitized drop profile is excellent as shown in Fig. 7.

The precision of the experiment, ca. 0.5%, is quite remarkable considering

that only 21 data points were used and that the comparison algorithms described

herein were designed specifically for execution on a microcomputer. More

sophisticated algorithms based upon extensions of these same concepts of shape

analysis can easily be developed for implementation with more powerful main

frame computers. Such improvements will undoubtedly increase the precision of

future interfacial tension measurements. In addition, improved computation

rates may enable the future study of transient interfacial phenomena.

Summary

   A novel method for the analysis of interfacial tension from the shape of
pendant fluid drops is presented. The experimental apparatus employs digital
video image processing techniques to record drop images and to segment the fluid
drop profile. An associated drop profile shape analysis algorithm is developed
based upon robust shape comparison methods that utilize repeated median con-
cepts. The complete algorithm is designed specifically to be executable on a
microcomputer. The performance of the algorithm is illustrated for simulated
pendant fluid drop profiles and pendant drops of glycerin. In the latter
case, the experimental precision in the resultant surface tension is found to be
of the order of 0.5%.

References

1. Padday, J. F. in "Surface and Colloid Science" (E. Matijevic, Ed.) Vol. I, pp. 101-149, Wiley, New York, 1969.

2. Ambwani, D. S., Fort, T., Jr., in "Surface and Colloid Science (R. J. Good and R. R. Stromberg, Eds.) Vol. II, pp. 93-119, Wiley, New York, 1979.

3. Neumann, A. W. and Good, R. J. in "Surface and Colloid Science" (R. J. Good and R. R. Stromberg, Eds.) Vol. II, pp. 31-91, Wiley, New York, 1979.

4. Gouy, G., C. R. Acad. Sci., $\underline{146}$, 1374 (1908).

5. Gouy, G., Ann. Phys., $\underline{6}$, 5 (1916).

6. Andreas, J. M., Hauser, E. A. and Tucker, W. B., J. Phys. Chem., $\underline{42}$, 1001 (1938).

7. Fordham, S., Proc. Roy. Soc. (London), $\underline{A194}$, 1 (1948).

8. Stauffer, C. J., J. Phys. Chem., $\underline{69}$, 1933 (1965).

9. Harland, S. and Hartley, R. W., "Axisymmetric Fluid-Liquid Interfaces", Elsevier, Amsterdam, 1976.

10. Roe, R.-J., Bachetta, V. L. and Wong, P. M. G., J. Phys. Chem., $\underline{71}$, 4190 (1967).

11. Boyce, J. F. Schürch, R., Rotenberg, Y. and Neumann, A. W., Colloids and Surfaces, $\underline{9}$, 307 (1984).

12. Bhatia, Q. S., Chen, J.-K., Koberstein, J. T., Sohn, J. E. and Emerson, J. A., J. Colloid Interface Sci., $\underline{106}$(2), 353 (1985).

13. Anastasiadis, S. H., Chen, J.-K., Koberstein, J. T., Sohn, J. E. and Emerson, J. A., Polym. Eng. Sci., to appear.

14. Girault, H. H., Schiffrin, D. J. and Smith, B. D. V., J. Electroanal. Chem., $\underline{137}$, 207 (1982).

15. Girault, H. H., Schiffrin, D. J. and Smith, B. D. B., J. Colloid Interface Sci., $\underline{101}$, 257 (1984).

16. Rotenberg, Y., Boruvka, L. and Neumann, A. W., J. Colloid Interface Sci., $\underline{93}$, 169 (1983).

17. Huh, C. and Reed, R. L., J. Colloid Interface Sci., $\underline{91}$, 472 (1983).

18. Siegel, A. F., Biometrica, $\underline{69}$, 242 (1982).

19. Olshan, A. F., Siegel, A. F. and Swindler, D. R., American J. Phy. Anthropology, $\underline{59}$, 131 (1982).

20. Siegel, A. F. nd Benson, R. H., Biometrics, $\underline{38}$, 341 (1982).

21. Castleman, K. R., "Digital Image Processing", Prentice-Hall, Englewood Cliffs, NJ (1979).

22. Pavlidis, T., "Algorithms for Graphics and Image Processing", Computer Science Press, Rockville, MD (1982).

23. Pavlidis, T., "Structural Pattern Recognition", Springer-Verlag, Berlin, Heidelberg (1977).

24. Kirsch, R. A., Computers and Biomedical Research, $\underline{4}$, 315 (1971).

25. Abdou, I. E. and Pratt, W. K., IEEE Proceedings $\underline{67}$, 753 (1979).

26. Hazlett, R. D., Schechter, R. S. and Aggarwal, J. K., Ind. Eng. Chem. Fundam., $\underline{24}$, 101 (1985).

27. "Chemical Engineers' Handbook", 5th edition, Perry, R. H. and Chilton, O. H., Eds., McGraw Hill, New York (1973).

28. "CRC Handbook of Chemistry and Physics", 4th edition, Weast, R. C., ed., CRC Press, Boca Raton, FL (1983).

Figure Captions

Fig. 1   Experimental geometry of pendant drop experiment.

Fig. 2   Block diagram of pendant drop apparatus.

Fig. 3   Typical digitized drop images

Original grey level image (left);

Thresholded binary image (center);

Segmented drop profile (right).

Fig. 4   Simulated pendant drop profile. (Dimensionless shape parameter B =

0.6)

Runge-Kutta solution of [1] (solid lines); points are simulated

integer number profiles with Gaussian random error (left); with

Gaussian random error, non-random error, and a one degree counter-

clockwise rotation (right).

Fig. 5   Effect of rotationally resistant smoothing with translation to the

origin.

Points are profiles with Gaussian random error (left); with Gaussian

random error, non-random error, and rotation (right); Solid lines are

the results of smoothing.

Fig. 6   Sum of squared residuals as a function of the dimensionless shape para-

meter for profiles simulated for B = 0.6. Circles: analysis without

smoothing; Open squares: analysis with rotationally resistant

smoothing; Filled squares: analysis with rotationally resistant

smoothing incorporating translation to the origin.

Analyis of profile with Gaussian random error (left);

Analysis of profile with Gaussian random error, non-random error and

rotation (right).

Fig. 7   Digitized pendant drop images of glycerin at room temperature (24.2°C).

Solid lines are the theoretical profiles obtained by application

of the algorithm.

Data points are the selected experimental data points (left);

Data points are the original segmented experimental drop profile
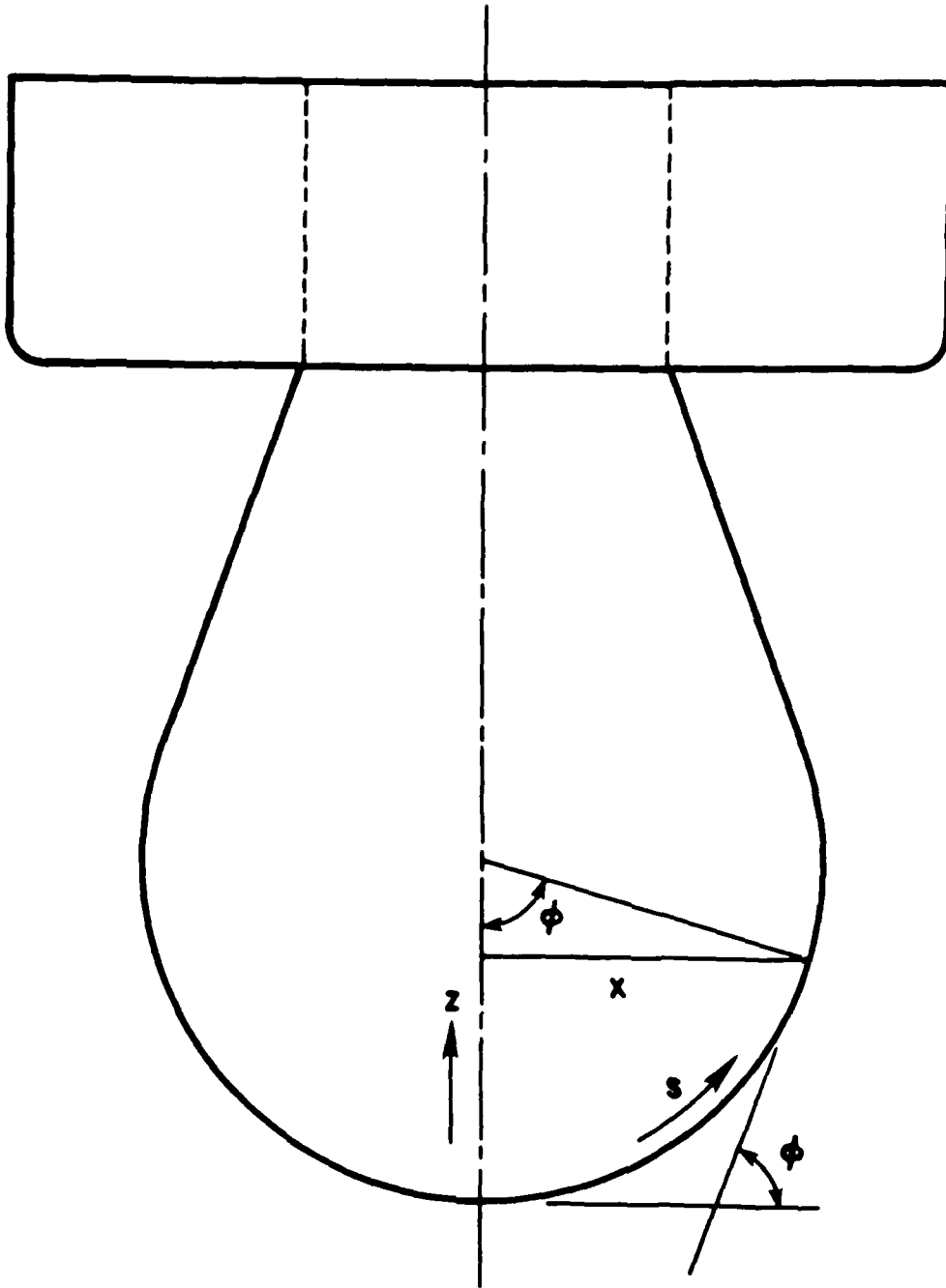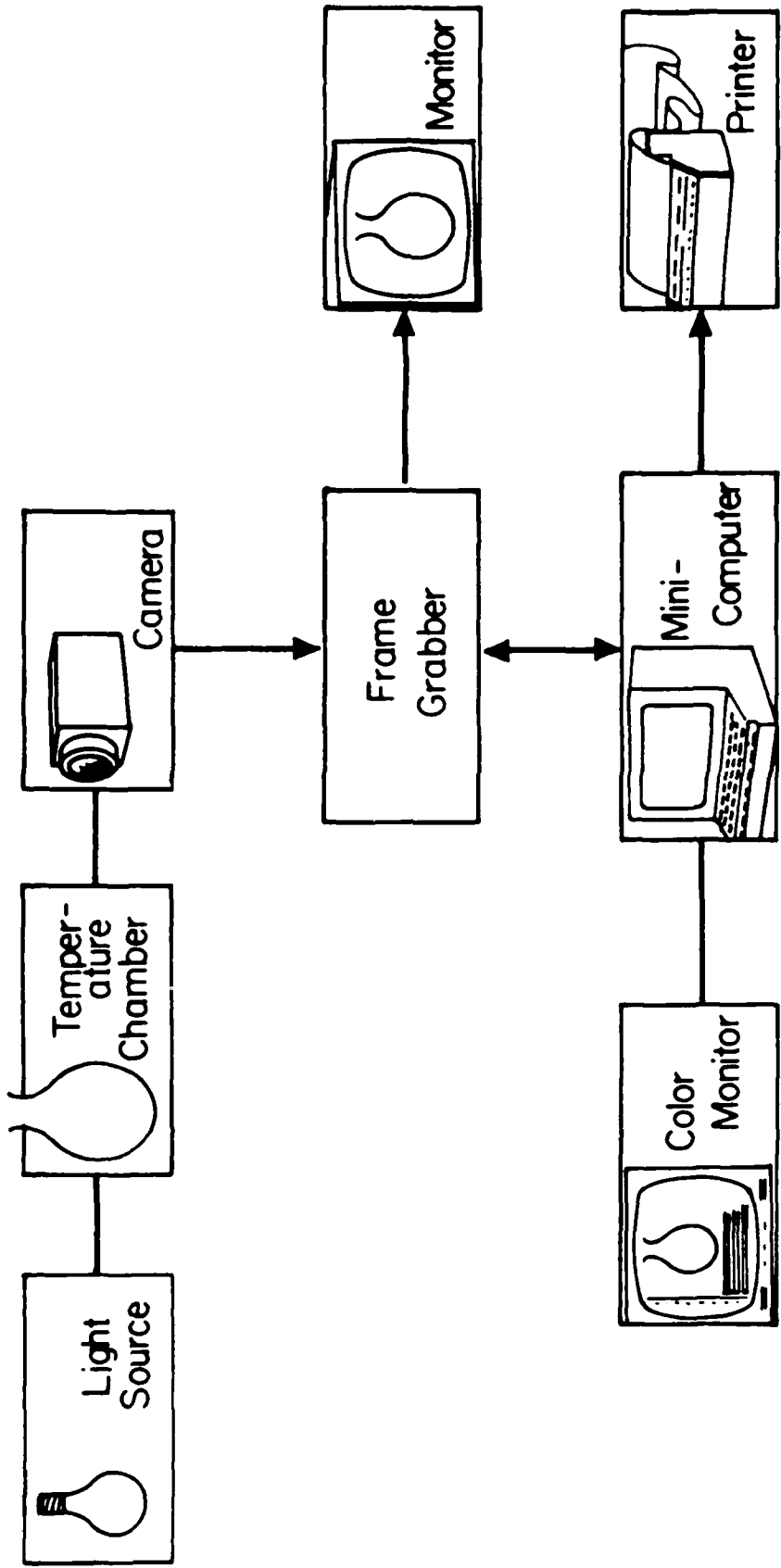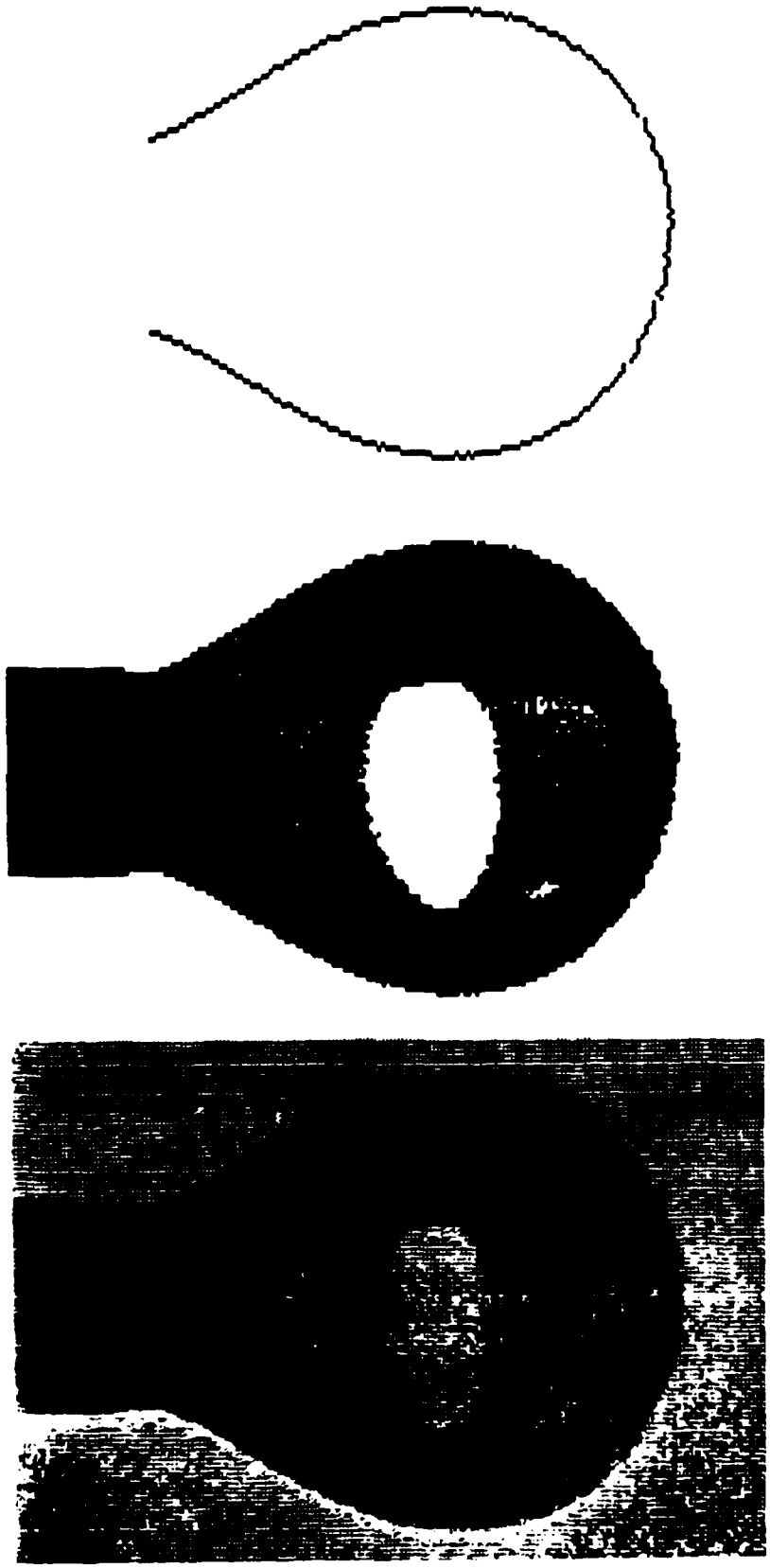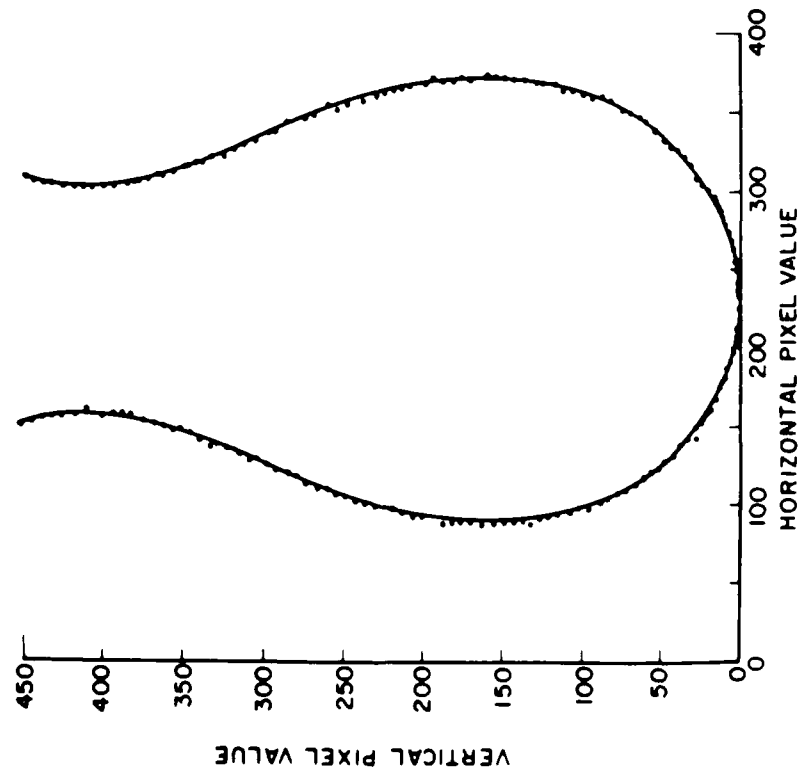
(right).

Fig. 1

Fig. 2

Fig. 3

Fig. 4

VERTICAL PIXEL VALUE

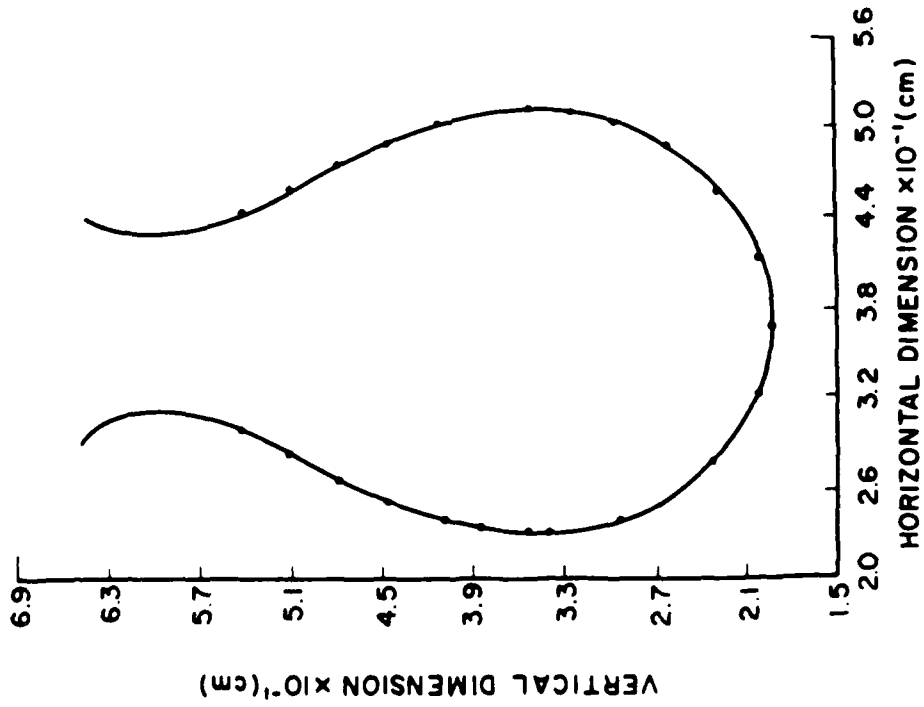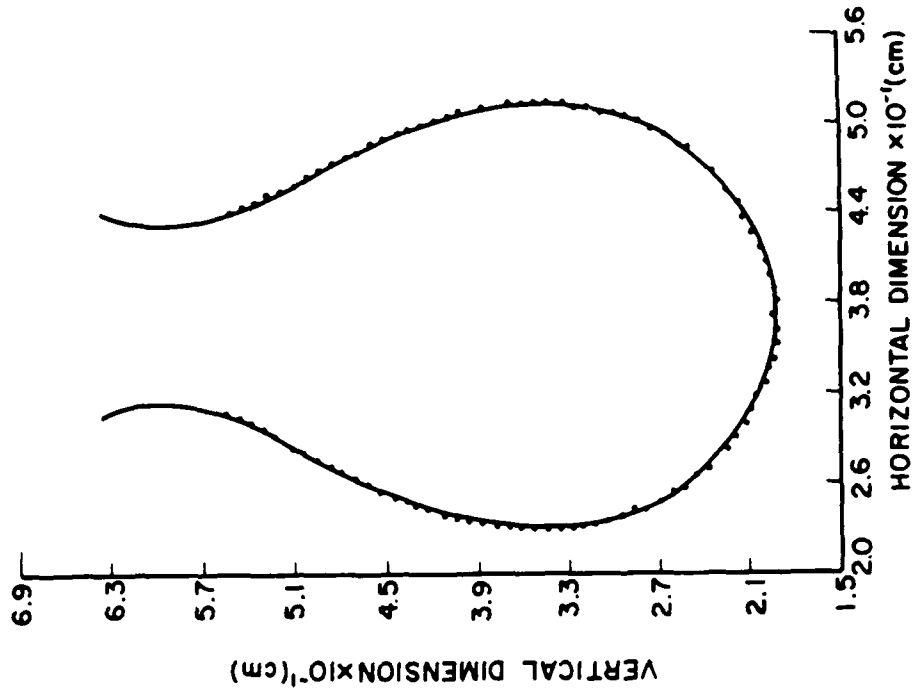HORIZONTAL PIXEL VALUE

VERTICAL PIXEL VALUE

HORIZONTAL PIXEL VALUE

Fig. 5

Fig. 6

Fig. 7

END
FILMED
4-86
DTIC